Momentum transport in the vicinity of q_{min} in reverse shear tokamaks due to ion temperature gradient turbulence

Rameswar Singh,[1,2,a] R Singh,[1,3] Hogun Jhang,[3] and P. H. Diamond[3,4,5]
[1]*Institute for Plasma Research, Bhat, Gandhinagar 382 428, India*
[2]*Laboratoire de Physique des Plasmas, Ecole Polytechnique route de Saclay, 91128 Palaiseau Cedex, France*
[3]*WCI Center for Fusion Theory, National Fusion Research Institute, Daejeon 305-333, South Korea*
[4]*Center for Momentum Transport and Flow Organization, University of California, San Diego, California 92093, USA*
[5]*Center for Astrophysics and Space Sciences, University of California San Diego, 9500 Gilman Dr., La Jolla, California 92093-0424, USA*

(Received 23 October 2013; accepted 20 December 2013; published online 13 January 2014; publisher error corrected 3 March 2014)

We present an analytic study of momentum transport of tokamak plasmas in the vicinity of minimum safety factor (q) position in reversed magnetic shear configuration. Slab ion temperature gradient modes with an equilibrium flow profile are considered in this study. Quasi-linear calculations of momentum flux clearly show the novel effects of q-curvature on the generation of intrinsic rotation and mean poloidal flow without invoking reflectional symmetry breaking of parallel wavenumber ($k_\parallel$). This q-curvature effect originates from the inherent asymmetry in $k_\parallel$ populations with respect to a rational surface due to the quadratic proportionality of $k_\parallel$ when q-curvature is taken into account. Discussions are made of possible implications of q-curvature induced plasma flows on internal transport barrier formation in reversed shear tokamaks. © *2014 AIP Publishing LLC*. [http://dx.doi.org/10.1063/1.4861625]

I. INTRODUCTION

Understanding of turbulent momentum transport in tokamak plasmas has been a key research topic over the past decades. This is because of the profound influence of plasma flows (both toroidal and poloidal) on confinement properties of tokamak plasmas. Radial transport of toroidal flow determines the flow profile which has an influence on confinement enhancement by providing the $E \times B$ shear driven by the radial flow gradient.[1,2] Plasma rotation can also stabilize dangerous, magnetohydrodynamics (MHD) instabilities such as resistive wall modes (RWM), which is essential to realize high performance advanced tokamak operation.[3,4]

Either external sources, such as neutral beam injection (NBI), or background turbulence (via turbulent Reynolds stress[5,6]) can drive plasma flows in tokamaks. The latter, known as *intrinsic rotation*,[7] has been a focus in confinement physics research for many years because of its potential impact on reactor scale experiments where neutral beams cannot penetrate into the core region. One of the mechanisms of intrinsic rotation generation is by conversion of radial inhomogeneity into $\langle k_\parallel \rangle$ (=spectrally averaged wavenumber in parallel direction) asymmetry driving residual stress.[8] Since background turbulence also gives rise to turbulent momentum diffusivity (viscosity), momentum convection/pinch, as well as playing as a source of intrinsic torque, the final flow profile will be determined by a "balance" between external and intrinsic torques and turbulent momentum conduction and pinch. Momentum pinch itself cannot drive intrinsic rotation; however, it is important for flow profile shaping. Symmetry breaking due to magnetic field curvature and gradient results in momentum pinch in tokamaks.[9–14]

Conversion of radial inhomogeneity into $\langle k_\parallel \rangle$ asymmetry requires some *symmetry breaking* mechanisms.[7,8,15–19] Role of mean $E \times B$ shearing in symmetry breaking, hence in off-diagonal momentum flux, was identified by many authors.[16,18] Recently, Gürcan *et al.* showed how the mean $E \times B$ shear can lead to the reflectional symmetry breaking of $\langle k_\parallel \rangle$ in ion temperature gradient (ITG) turbulence, resulting in finite parallel residual stress.[18] Reflectional symmetry breaking of $k_\parallel$ here means generation of eigenmode averaged wave number $\langle k_\parallel \rangle \neq 0$ by symmetry breaking of eigenmode about a rational surface, i.e., by $|\phi|^2(x) \neq |\phi|(-x)$. Turbulence intensity gradient can also induce $\langle k_\parallel \rangle$ symmetry breaking,[19] which may be an important driver of the intrinsic torque near the top of a transport barrier where a strong fluctuation intensity gradient is present. The process of $\langle k_\parallel \rangle$ symmetry breaking by $E \times B$ shear and/or intensity gradient implies a coupling between intrinsic rotation and transport barrier dynamics, such as internal transport barrier (ITB) formation, which involves steep temperature and/or density gradients (i.e., strong radial inhomogeneity) and the strong $E \times B$ shear and/or the fluctuation intensity gradient (i.e., $\langle k_\parallel \rangle$ symmetry breaking). Gyrokinetic simulations have shown the generation of intrinsic rotation from the $\langle k_\parallel \rangle$ symmetry breaking by mean $E \times B$ shear[20–23] and turbulence intensity gradient[20] and up-down asymmetry of equilibrium magnetic topology.[24,25] Gyrokinetic simulations have also shown residual stress from profile shearing effects.[26,27]

Apart from the symmetry breaking driven by mean $E \times B$ shear, turbulence can also generate mean poloidal and parallel flows via various other mechanisms. Weiland *et al.*[28] showed toroidal residual stress generation form by

[a]rameswar@ipr.res.in

toroidicity using a fluid theoretical calculation. McDevitt *et al*. showed from a gyrokinetic analysis that polarization drift may drive intrinsic rotation.[29,30] The residual stress induced by polarization drift does not require $E \times B$ shear. This was confirmed by Singh *et al*. who calculated radial quasi-linear fluxes of toroidal and poloidal momentum from a fluid formulation of ITG turbulence.[31] They also showed that polarization drift does not generate poloidal Reynolds stress. A density gradient can also generate parallel residual stress by producing a shift of eigenmodes due to finite ρ_s^*.[32] The ρ_s^* term originates from the divergence of a polarization current when an equilibrium density gradient is present. Due to the development of a strong density gradient at transport barriers, this may be active at transport barriers. Regarding on poloidal flow generation, Singh *et al*. propose that "$\langle k_x \rangle$ symmetry breaking" (k_x is the radial wavenumber) induces residual poloidal stress. Specifically, they showed that mean *parallel* flow shear can drive poloidal Reynolds stress by making spectrally averaged $\langle \mathrm{Re} k_x \rangle$ finite.[31] This suggests a coupling of parallel and poloidal flow dynamics. For an overview of toroidal momentum transport theories and phenomenology, the readers are referred to Refs. 33–35.

We note that all previous studies on turbulence induced residual stress have been made in monotonic shear profiles, which possess inherent $\langle k_\| \rangle$ symmetry. It is desirable to study turbulent momentum transport in reversed shear (RS) configuration because:

- The presence of q-profile curvature brings about inherent $\langle k_\| \rangle$ asymmetry due to the relation, $k_\| \sim s_d x^2$, where s_d is the q-profile curvature and x is the distance from the rational surface. A recent gyrokinetic simulation clearly shows the effects of q-profile curvature on intrinsic rotation generation by this mechanism.[22]
- Reversed shear configuration promotes ITB formation the dynamics of which is strongly coupled to momentum transport.

It is likely that the first point may shed light on the possible interpretation of recent Alcator C-mod experiments, showing a clear change of intrinsic torque when lower hybrid (LH) waves are applied.[36] We expect that the q-curvature effects will become important as strong LH waves are injected, leading to higher intrinsic torque, as will be shown in this paper. Regarding on the second point, the combined role of the q-profile shape and momentum transport in ITB dynamics has been observed in tokamak experiments where ion ITB formation is facilitated when sufficiently strong external torque is delivered by NBI[37] or strong intrinsic rotation is generated.[38] Recent gyrofluid simulations have clearly shown the coupling of momentum transport and intrinsic rotation to the ITB dynamics (i.e., formation and back transitions of an ITB and intrinsic rotation-external torque interaction) in RS configuration.[39,40]

The q-curvature effect can be classified as an element of profile shearing effect. The effect of profile shearing is two fold: (1) to produce gradient in turbulence intensity[19] which can cause residual stress by $k_\|$ symmetry breaking that acts at pressure profile curvature region. (2) Eigenmode tilt about the low field side mid-plane $\theta = 0$,[41–43] which has shown to cause residual stress in global gyrokinetic simulations.[27] Partial inclusion of profile shear as diamagnetic velocity shear in local flux tube formulation has also revealed residual stress by profile shear.[26] This effect can also be captured as radial eigenmode asymmetry about a mode rational surface $x = 0$ in simple sheared slab geometry in fluid formulation. q-curvature being one of the element of profile shearing effects may contribute to turbulence intensity inhomogeneity not the sole creator of it though. Also q-curvature is not expected to cause eigenmode asymmetry as can be seen in sheared slab calculations. So q-curvature can alter residual stress in an indirect way via turbulence intensity gradient. The direct effect of q-curvature is via the x^2 dependence of $k_\|$ which ultimately produces residual stress depending on mode width when turbulence intensity is homogeneous and eigenmode is symmetric. If turbulence intensity gradient is present then one piece of residual stress comes from the x dependence of $k_\|$ and the residual stress depends on mode width. q-curvature via x^2 dependence of $k_\|$ and turbulence intensity gradient can synergistically add a piece of residual stress provided the eigenmode is asymmetric about $x = 0$ which can come from E × B shear and/or from pressure profile shear (i.e., pressure curvature). Near q-min at ITB in reverse shear configuration the pressure curvature is weak and hence turbulence intensity gradient is very weak, giving an opportunity to cleanly and clearly see the q-curvature effect.

In this paper, we study turbulent momentum transport in RS profile. Specifically, we calculate the effects of q-profile curvature on turbulent viscosity and parallel and poloidal Reynolds stresses. ITB exist near q-min in the reverse shear configuration where temperature and density gradients are steep. So curvature effects are expected to be small. Toroidal mode coupling is also weak in a small magnetic shear region around the qmin-surface. Moreover, a negative magnetic shear has strong stabilizing effect on toroidal ITG at low q values,[44,45] whereas slab ITG growth is independent of sign of magnetic shear. Further ITG mode exhibit a slab-like feature in the negative-sheared magnetic configuration as shown by a gyrokinetic pseudospectral global code GLOGYSTO.[46] So ITG modes in sheared slab geometry are considered in this work. As mentioned before, the presence of q-curvature inherently break the $\langle k_\| \rangle$ symmetry, leading to net parallel momentum generation without regard to the $E \times B$ symmetry breaking mechanism. The amount of net momentum generated by the q-curvature effect is found to be proportional to the width of the mode, rather than the shift off the rational surface. This effect is particularly notable at minimum q-position where magnetic shear is zero and only the curvature term survives. In general, q-profile curvature contributes to all aspects of momentum transport, including turbulent viscosity, parallel and poloidal Reynolds stresses.

The rest of the paper is organized as follows. In Sec. II, we describe the basic formulation. We derive a linear dispersion relation for ITG modes in the presence of q-profile curvature. In Sec. III, we calculate eigenmode structures of unstable modes. Section IV is devoted to quasi-linear calculations of momentum flux in the vicinity of q-minimum position. After introducing a formulation elucidating the effects

of q-curvature, we calculate parallel and poloidal Reynolds stresses. A particular emphasis is put on the effects of q-curvature and discussions are made of their possible implications on ITB formation. We conclude this paper in Sec. V with a brief summary of main results and some discussions.

II. FORMULATION

We start from a description of a magnetic field near the minimum value of safety factor (q_{min}) in reversed magnetic shear configuration[47]

$$\vec{B} = B\left(\hat{z} - \frac{\hat{s}x}{q_0 R}\left(1 + \frac{\hat{s}_d x}{\hat{s}}\right)\hat{y}\right), \tag{1}$$

where $\hat{s} = rq_0'/q_0$ and $\hat{s}_d = rq_0''/2q_0$ are the shear and the curvature of q, respectively, $q_0 = q_{min}$ is the q-value at $r = r_0$ with r_0 being the radial position of a reference surface. q_0 is not necessarily a rational number. Sheared slab geometry is employed in this paper. The prime and double prime represent the first and second derivatives, respectively, with respect to $x \equiv r - r_0$. From Eq. (1), $k_\parallel$ becomes

$$k_\parallel = k_z - \frac{k_y \hat{s} x L_n}{q_0 R}\left(1 + \frac{\hat{s}_d x}{\hat{s}}\right). \tag{2}$$

In Eq. (2), we normalize $k_\parallel$ and k_z to L_n and k_y, x, $\hat{s}_d$ to ρ_s (i.e., $(k_\parallel, k_z) \equiv (k_\parallel, k_z)L_n$, $(k_y, \hat{s}_d) \equiv (k_y, \hat{s}_d)\rho_s$ and $x \equiv x/\rho_s$).

In this study, we consider the fluid ITG instability. The model equations to describe this instability consist of the conservation of perturbed ion density, parallel momentum, and pressure,[31,32,48,49]

$$\left(\frac{\partial}{\partial t} + x\hat{V}_{E0}'\nabla_y\right)\left(1 - \nabla_\perp^2 + \frac{\rho_s}{L_n}\nabla_x\right)\phi + \left[1 + K\left(\nabla_\perp^2 - \frac{\rho_s}{L_n}\nabla_x\right)\right]\nabla_y\phi + \nabla_\parallel v = 0, \tag{3}$$

$$\left(\frac{\partial}{\partial t} + x\hat{V}_{E0}'\nabla_y\right)v - \hat{V}_{\parallel 0}'\nabla_y\phi + \nabla_\parallel(p + \phi) = 0, \tag{4}$$

$$\left(\frac{\partial}{\partial t} + x\hat{V}_{E0}'\nabla_y\right)p + K\nabla_y\phi + \Gamma\nabla_\parallel v = 0. \tag{5}$$

The various quantities in Eqs. (3)–(5) are normalized as $x = (x - x_0)/\rho_s, y = y/\rho_s, z = z/L_n, t = tc_s/L_n, \phi = (e\delta\phi/T_e)$ (L_n/ρ_s), $n_i = (\delta n_i/n_0)(L_n/\rho_s)$, $v = (\delta v_{\parallel i}/c_s)(L_n/\rho_s)$, $p = (\tau_i \delta p_i/P_{i0})$ (L_n/ρ_s), and $L_n\nabla_\parallel \equiv \nabla_\parallel = \frac{\partial}{\partial z} + xs\frac{\partial}{\partial y}$ with $L_n^{-1} = -\nabla n_0/n_0$ being the equilibrium density scale length, $c_s = \sqrt{T_{e0}/m_i}$, $\rho_s = c_s/\Omega_i$ being the ion-acoustic Larmor radius, and $\tau_i = T_{0i}/T_{0e}$ being the ratio of equilibrium ion to electron temperature. Also, various dimensionless parameters are defined as $\eta_i = L_n/L_T$ with $L_T^{-1} = -\nabla T_{0i}/T_{0i}$ the equilibrium ion temperature scale length, $K = \tau_i(1 + \eta_i) = \tau_i\alpha_i$, $\Gamma = \gamma\tau_i$, with γ being the adiabatic index, $s = L_n/L_s$, $\hat{V}_{E0}' = (L_n/c_s)V_{E0}'$, and $\hat{V}_{\parallel 0}' = (L_n/c_s)V_{\parallel 0}'$, where V_{E0}' and $V_{\parallel 0}'$ are equilibrium $E \times B$ and parallel flow shear, respectively. In Eq. (3), we keep $\rho_s^* = \rho_s/L_n$ terms following Ref. 20. These terms come from the divergence of polarization current in the presence of equilibrium density gradient, separately from the standard vorticity term. Usually, they are small in the standard drift wave ordering. However, they may be considerable inside ITBs due to a strong density gradient there.

Now, we consider perturbations of the form $f = f_k(x)\exp(ik_y y + ik_z z - i\omega t)$, where ω is normalized to c_s/L_n, $\omega = \omega/(c_s/L_n)$. Then, one can derive the following eigenvalue equation in ϕ_k from Eqs. (3)–(5):

$$\frac{d^2\phi_k}{dx^2} - \rho_s^*\frac{d\phi_k}{dx} + U(x, \Omega)\phi_k = 0, \tag{6}$$

where

$$U(x, \Omega) = -k_y^2 + \frac{1 - \hat{\Omega}}{K + \hat{\Omega}} + \frac{(k_\parallel/k_y)^2(K + \hat{\Omega}) - (k_\parallel/k_y)\hat{\Omega}\hat{V}_\parallel'}{(K + \hat{\Omega})\left(\hat{\Omega}^2 - \Gamma(k_\parallel/k_y)^2\right)}, \tag{7}$$

with the definitions $\hat{\Omega} = \Omega - x\hat{V}_E'$, $\hat{V}_{E,\parallel}' = L_n V_{E,\parallel}'/c_s$, $\Omega = \omega/k_y$, and $\omega_{*e} = c_s k_y/L_n$. Equation (7) represents a general form for the effective potential in the presence of q-profile curvature. When $\Gamma \to 0$ and $E \times B$ shearing rate is much smaller than the mode frequency, Eq. (7) becomes

$$U(x, \Omega) = A_0 + A_1 x + A_2 x^2 + A_3 x^3 + A_4 x^4, \tag{8}$$

where

$$A_0 = -k_y^2 + \frac{k_y - \omega}{Kk_y + \omega} + \frac{k_z^2}{\omega^2} - \frac{k_y k_z \hat{V}_\parallel'}{\omega(Kk_y + \omega)},$$

$$A_1 = \left(k_y\frac{\hat{V}_E'}{Kk_y + \omega} - \frac{1}{\omega^2}\frac{2k_y k_z \hat{s} L_n}{q_0 R}\right) + \frac{k_y}{\omega(Kk_y + \omega)}\frac{k_y \hat{s} L_n \hat{V}_\parallel'}{q_0 R},$$

$$A_2 = \frac{1}{\omega^2}\left\{\left(\frac{k_y \hat{s} L_n}{q_0 R}\right)^2 - \frac{2k_y k_z \hat{s}_d L_n}{q_0 R}\right\} + \frac{k_y}{\omega(Kk_y + \omega)}\frac{k_y \hat{s}_d L_n \hat{V}_\parallel'}{q_0 R},$$

$$A_3 = \frac{1}{\omega^2}\frac{k_y \hat{s} L_n}{q_0 R}\frac{2k_y \hat{s}_d L_n}{q_0 R},$$

$$A_4 = \frac{1}{\omega^2}\left(\frac{k_y \hat{s}_d L_n}{q_0 R}\right)^2.$$

To make a further analytical progress, we keep terms up to x^2 in Eq. (8). A higher order calculation keeping the higher order terms can be made by using a perturbation method, as will be described in Sec. III. Defining a new coordinate variable,

$$\xi = (-A_2)^{1/4}\left(x + \frac{A_1}{2A_2}\right) \tag{9}$$

and following the methodology in Ref. 20, one can show that Eq. (6) becomes a Weber's equation

$$\frac{d^2\phi_k}{d\xi^2} - (-A_2)^{-1/4}\rho_s^*\frac{d\phi_k}{d\xi} + (E - \xi^2)\phi_k = 0, \tag{10}$$

where $E = (A_0 - \frac{A_1^2}{4A_2})/\sqrt{(-A_2)}$. If we define a new potential variable Φ_k as

$$\phi_k = \Phi_k \exp\left(\frac{1}{2}\int(-A_2)^{-1/4}\rho_s^* d\xi\right), \tag{11}$$

the first derivative term in Eq. (10) can be removed. Then, Eq. (10) reduces to a simpler form

$$\frac{d^2\Phi_k}{d\xi^2} + \left(E^* - \xi^2\right)\Phi_k = 0, \tag{12}$$

where

$$E^* = E - \left(\frac{(-A_2)^{-1/4}\rho_s^*}{2}\right)^2. \tag{13}$$

Solutions of Eq. (12) are well-known and given by

$$\Phi_{kl} = \Phi_0 \exp\left(-\frac{\xi^2}{2}\right) H_l(\xi), \tag{14}$$

with

$$E^* = 2l + 1, \quad l = 0, 1, 2, 3, ... \tag{15}$$

Here, $H_l(\xi)$ is the l-th order Hermite polynomial. We consider the most dominant, lowest order mode (i.e., $l = 0$) for which the eigenfunction is

$$\Phi_k = \Phi_0 \exp\left[-\frac{1}{2} i\sqrt{A_2}\left(x + \frac{A_1}{2A_2}\right)^2\right]. \tag{16}$$

Then, the corresponding eigenfunction ϕ_k, Eq. (11), becomes

$$\phi_k = \Phi_0 \exp\left[-\frac{1}{2} i\sqrt{A_2}\left(x + \frac{A_1}{2A_2}\right)^2\right] \exp\left[\frac{1}{2}\rho_s^*\left(x + \frac{A_1}{2A_2}\right)\right]. \tag{17}$$

Equation (17) clearly shows that the eigenfunction is shifted off the mode rational surface due to finite ρ_s^*, even in the absence of equilibrium shear flow. Making use of the eigenvalue relation, Eq. (13),

$$1 = \frac{\left(A_0 - \frac{A_1^2}{4A_2}\right)}{\sqrt{(-A_2)}} - \left(\frac{(-A_2)^{-1/4}\rho_s^*}{2}\right)^2$$

leads to the following dispersion relation corresponding to the lowest order eigenfunction:

$$\begin{aligned} &-k_y^2 + \frac{1-\Omega}{K+\Omega} + \frac{k_z^2}{k_y^2\Omega^2} - \frac{k_z\hat{V}_\parallel'}{k_y\Omega(K+\Omega)} \\ &- \frac{1}{4}\left\{\frac{\hat{V}_E'}{K+\Omega} - \frac{1}{k_y^2\Omega^2}\frac{2k_yk_z\hat{s}L_n}{q_0R} + \frac{1}{k_y\Omega(K+\Omega)} \right. \\ &\left. \times \frac{k_y\hat{s}L_n\hat{V}_\parallel'}{q_0R}\right\}^2 \left[\frac{1}{k_y^2\Omega^2}\left\{\left(\frac{k_y\hat{s}L_n}{q_0R}\right)^2 - \frac{2k_yk_z\hat{s}_dL_n}{q_0R}\right\} \right. \\ &\left. + \frac{1}{k_y\Omega(K+\Omega)}\frac{k_y\hat{s}_dL_n\hat{V}_\parallel'}{q_0R}\right]^{-1} - \left(\frac{\rho_s^*}{2}\right)^2 = i\left\{\frac{1}{k_y^2\Omega^2}\left(\left(\frac{k_y\hat{s}L_n}{q_0R}\right)^2 \right. \right. \\ &\left. \left. - \frac{2k_yk_z\hat{s}_dL_n}{q_0R}\right) + \frac{1}{k_y\Omega(K+\Omega)}\frac{k_y\hat{s}_dL_n\hat{V}_\parallel'}{q_0R}\right\}^{1/2}. \end{aligned} \tag{18}$$

One may rewrite Eq. (17) as

$$\phi_k = \Phi_0 \exp\left[-\frac{1}{2} i\sqrt{A_2}\left(x + \frac{A_1}{2A_2} - \frac{\rho_s^*}{2\sqrt{-A_2}}\right)^2\right] \times \exp\left[i\frac{1}{2}\sqrt{A_2}\left(\frac{\rho_s^*}{2\sqrt{-A_2}}\right)^2\right]. \tag{19}$$

Separation of the real (Re) and imaginary (Im) parts of the phases in Eq. (19) yields a further useful form of the eigenfunction

$$\phi_k = \Phi_0 \exp\left[-\frac{1}{2}\left(\frac{x - \xi_{*k}}{\Delta_k}\right)^2\right] \exp\left[-i\frac{1}{2}\mathrm{Re}\sqrt{A_2} \times \left(x + \mathrm{Re}\frac{A_1}{2A_2} - \frac{\mathrm{Im}\sqrt{A_2}}{\mathrm{Re}\sqrt{A_2}}\mathrm{Im}\frac{A_1}{2A_2}\right)^2\right], \tag{20}$$

where

$$\xi_{*k} = -\left[\mathrm{Re}\frac{A_1}{2A_2} + \frac{\mathrm{Re}\sqrt{A_2}}{\mathrm{Im}\sqrt{A_1}}\mathrm{Im}\frac{A_1}{2A_2} + \frac{\rho_s^*}{2\mathrm{Im}\sqrt{A_2}}\right] \tag{21}$$

is the mode shift off the reference surface, and

$$\Delta_k^{-2} = -\mathrm{Im}\sqrt{A_2} \tag{22}$$

represents the half mode width. From Eqs. (20)–(22), it is clear that ρ_s^* gives rise to the mode shift, while it does not generate $\mathrm{Re}(k_x)$ of the mode. Note that the factor

$$\exp\left\{-\frac{i}{2}\sqrt{A_2}\left[\left(1 + \left(\frac{\mathrm{Re}\sqrt{A_2}}{\mathrm{Im}\sqrt{A_2}}\right)^2\right)\left(\mathrm{Im}\frac{A_1}{2A_2} + \frac{\rho_s^*\mathrm{Re}\sqrt{A_2}}{2|\sqrt{A_2}|^2}\right)^2 + \left(\frac{\rho_s^*}{2\sqrt{A_2}}\right)^2\right]\right\} \tag{23}$$

has been absorbed in the mode amplitude Φ_0 in writing Eq. (20). It indicates that a turbulence intensity gradient naturally arises because A_1 and A_2 contain mean plasma profiles. This intensity gradient can lead to $k_\parallel$ symmetry breaking, resulting in the generation of intrinsic rotation.[19]

III. EIGENMODE STRUCTURE

In tokamaks, an (m, n) mode (m and n are poloidal and toroidal mode numbers, respectively) can have one or more resonant surfaces depending on the q-profile under consideration. In RS configuration, the (m, n) mode has one or two resonant surfaces where $q(r) = m/n$ is satisfied. Figure 1 shows a typical RS profile and position of rational surfaces resonating with $n = 2$. In this particular case, $2 \le m \le 3$ modes have two resonant surfaces. Only one resonant surface exists for higher m modes (higher than $m = 11$). In this paper, we focus on double resonant modes which are excited when q_{min} is an irrational number and involve two resonant surfaces. Application of the same methodology to single resonant modes (i.e., q_{min} is a

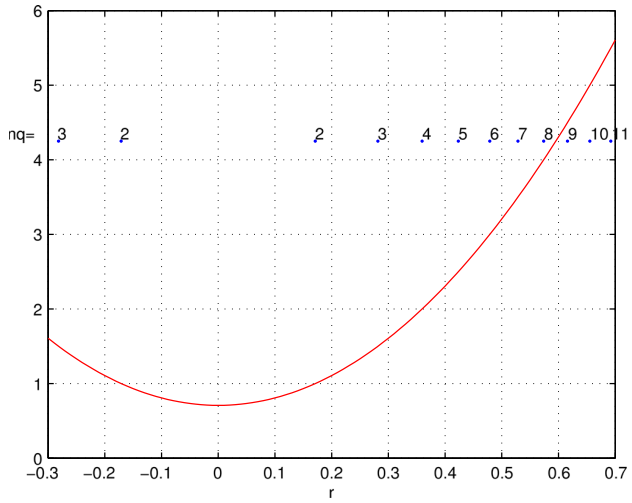

FIG. 1. A reverse q-profile and position of rational surfaces resonating with the toroidal mode number $n=2$. Zero at the x-axis (radial coordinate) corresponds to the position of q_{min}. $q(r)=(q_{min}+c_1(r-c_2)^2)$ with $q_{min}=1/\sqrt{2}$, $c_1=10.0$, $c_2=0$. Here, $r\equiv r/a$ with a being the minor radius.

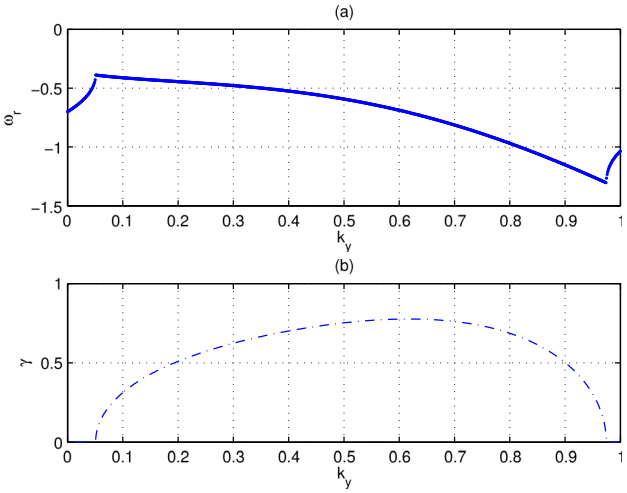

FIG. 2. Real (a) and imaginary (b) parts of the mode frequency vs. k_y of a double resonant mode. Parameters being used are $L_n=0.020\times 4\,\mathrm{m}$, $L_T=0.020\,\mathrm{m}$, $V_E'=0.0$, $V_\parallel'=0.0$, $\hat{s}=0.0$, $T_e=4.0$ keV, $T_i=4.0$ keV, $m_i=m_H=1.67\times10^{-27}$ kg, $B=4.6$ T, $r_0/a=0.3\,\mathrm{m}$, $q_0''=20$, $R=2.0\,\mathrm{m}$, $k_z=0.7$, and $\rho_s=1.40\times10^{-3}$ m.

rational number) is straightforward by setting $\hat{s}=0$ and $k_z=0$. If q_{min} is a irrational number (i.e., $q_{min}\neq m/n$), $k_z=(m-nq_{min})/qR\neq 0$. Then the mode has two rational surfaces on both sides of $r=r_{min}$. The position of these rational surfaces is given by quadratic roots of Eq. (2) with $\hat{s}=0$, resulting in $x_{res}=\pm\sqrt{(k_z/k_y)(q_0R/\hat{s}_dL_n)}$. Note that x_{res} is symmetric with respect to $r=r_{min}$ (i.e., $x=0$).

We first consider the simplest case when $\hat{V}_E'=\hat{V}_\parallel'=0$ at $r=r_{min}$. In fact, they can have maximum values at $r=r_{min}$, as shown in recent gyrofluid simulations.[50] This restriction will be relaxed later in this section. Then, it is easy to show that the lowest order eigenfunction becomes

$$\phi_k=\Phi_0\exp\left[-\frac{1}{2}\left(\frac{x-\xi_{*k}}{\Delta_k}\right)^2\right]\exp\left[-i\frac{1}{2}\mathrm{Re}\sqrt{A_2}x^2\right], \quad (24)$$

with

$$A_2=-\frac{2}{\omega^2}\frac{|k_yk_z|\hat{s}_dL_n}{q_0R},$$

$$\Delta_k^{-2}=-\mathrm{Im}\sqrt{A_2}=\frac{\omega_r}{|\omega|^2}\sqrt{\frac{2|k_yk_z|\hat{s}_dL_n}{q_0R}},$$

$$\xi_{*k}=-\frac{\rho_s^*}{2\mathrm{Im}\sqrt{A_2}}=\frac{\rho_s^*}{2}\Delta_k^2.$$

Again, the factor $\exp(-\rho_s^{*2}/2\mathrm{Im}\sqrt{A_2})$ has been absorbed in the amplitude Φ_0. Equation (24) represents an eigenmode with the envelope shifted from $x=0$. The mode width Δ_k scales as $\Delta_k\propto\hat{s}_d^{-1/4}$, implying further localization of the mode when q-curvature gets stronger. Note that ξ_{*k} in this case coincides with Δ_k ($\xi_{*k}\propto\Delta_k^2$) and comes entirely from finite ρ_s^* which may be considerable at $r=r_{min}$ in a reversed shear ITB.

From Eq. (18), one can easily obtain the dispersion relation corresponding to these modes

$$-k_y^2+\frac{k_y-\omega}{Kk_y+\omega}+\frac{k_z^2}{\omega^2}-\left(\frac{\rho_s^*}{2}\right)^2=\frac{1}{\omega}\left(\frac{2|k_yk_z|\hat{s}_dL_n}{q_0R}\right)^{1/2}. \quad (25)$$

Figures 2(a) and 2(b) show real (ω_r) and imaginary (γ) parts of the mode frequency as a function of k_y when $k_z=0.7$. To produce Fig. 2, we use the dispersion relation Eq. (25) with the parameters, $L_n=0.080\,\mathrm{m}$, $L_T=0.020\,\mathrm{m}$, $V_E'=V_\parallel'=0.0$, $\hat{s}=0.0$, $T_e=4.0\,\mathrm{keV}$, $T_i=4.0\,\mathrm{keV}$, $m_i=m_H=1.67\times10^{-27}\,\mathrm{kg}$, $B=4.6\,\mathrm{T}$, $r_{min}/a=0.3$, $q_0''=20$, $R=2.0\,\mathrm{m}$, and $\rho_s=1.40\times10^{-3}\,\mathrm{m}$. The growth rate is maximized and changes little in the range of $0.5\lesssim k_y\lesssim 0.7$. The lowest order eigenfunction for a growing mode is plotted in Fig. 3. The same plasma parameters as in Fig. 2 with $\omega_r=-0.672$ and

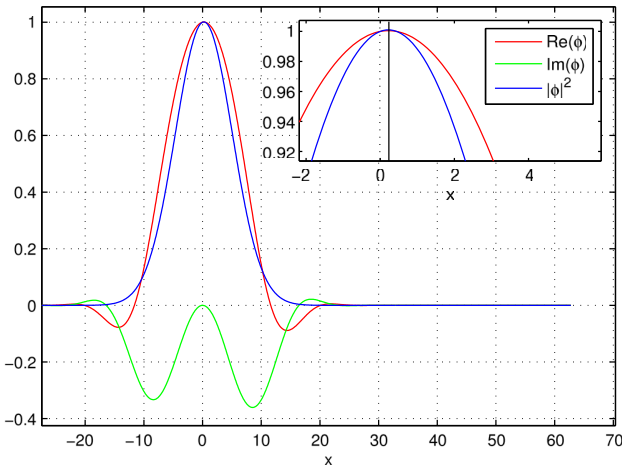

FIG. 3. The lowest order eigenfunction for a growing double resonant mode with $\omega=-0.672+i0.7745$. The solid vertical line in the inset indicates the mode shift off the reference surface due to ρ_s^*. Mode shift (ξ_{*k}) and width (Δ_k) are $\xi_{*k}=0.6485$ and $\Delta_k=8.0394$, respectively. The same plasma parameters as in Fig. 2 have been used.

$\gamma = 0.7745$ are used to produce Fig. 3. The mode shift due to ρ_s^* is highlighted in the inset of Fig. 3.

One can make a higher order correction of the eigenvalues and eigenfunctions by employing a perturbation method in a similar way to that being used in quantum mechanics. An example of this higher order calculation is presented in Appendix where we solve Eq. (6) perturbatively by keeping the quartic term in Eq. (8). Since $A_1 = A_3 = 0$ because $\hat{s} = 0$ and $\hat{V}_E^{'} = \hat{V}_{\parallel}^{'} = 0$ in this case, the potential is symmetric with respect to $x = 0$.

Now, we consider the general case when the minimum of E_r well does not coincide with $r = r_{min}$ position. For analytic tractability of the problem, we assume that the parallel flow shear is relatively weak in the sense that $-2k_z(Kk_y + \omega) \gg \omega k_y \hat{V}_{\parallel}^{'}$. Under this assumption, one can neglect the last term in the expression for A_2 in Eq. (8). This allows us to write the eigenfunction in the form of Eq. (20) with the mode shift including the ρ_s^* term

$$\xi_{*k} = -\frac{k_y^2 K \hat{V}_E^{'} |\omega|^2}{4|k_y k_z||Kk_y + \omega|^2} \frac{q_0 R}{\hat{s}_d L_n} - \frac{\rho_s^* |\omega|^2}{2\omega_r} \sqrt{\frac{q_0 R}{2|k_y k_z| \hat{s}_d L_n}}.$$

The dispersion relation in this case becomes

$$-k_y^2 + \frac{k_y - \omega}{Kk_y + \omega} + \frac{k_z^2}{\omega^2} + \frac{1}{4}\left(\frac{\omega k_y \hat{V}_E^{'}}{Kk_y + \omega}\right)^2 \left(\frac{q_0 R}{2|k_y k_z| \hat{s}_d L_n}\right) - \left(\frac{\rho_s^*}{2}\right)^2 = \frac{1}{\omega}\left(\frac{2|k_y k_z| \hat{s}_d L_n}{q_0 R}\right)^{1/2}. \quad (26)$$

Figures 4(a) and 4(b) show real (ω_r) and imaginary (γ) parts of the mode frequency as a function of k_y. We use the dispersion relation Eq. (26) with the same parameters as in Fig. 2 with $V_E^{'} = 0.01$. A comparison of Fig. 4(b) with Fig. 2(b) shows that the growth rate is significantly reduced due to $\hat{V}_E^{'}$, especially, in the high k_y region; complete

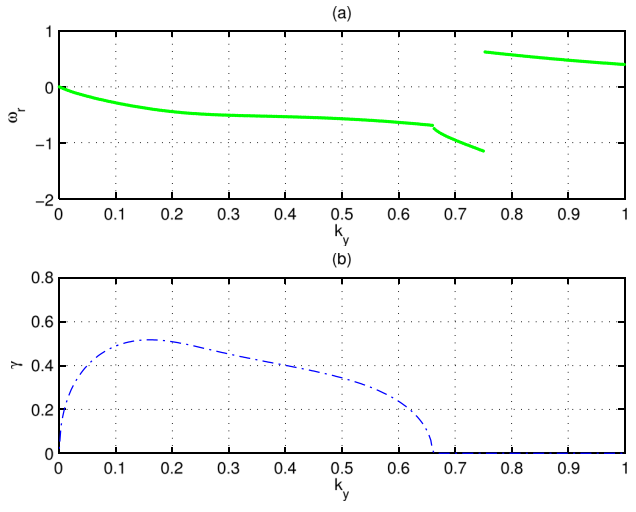

FIG. 4. Real (a) and imaginary (b) parts of the mode frequency vs. k_y of a double resonant mode with finite equilibrium $E \times B$ shear. The same parameters as in Fig. 2 have been used except $L_n = 0.019 \times 4$ m, $L_T = 0.019$ m, and $\hat{V}_E^{'} = 0.01$. Compared to Fig. 2, the growth rate is significantly reduced due to $\hat{V}_E^{'}$, especially in high k_y region.

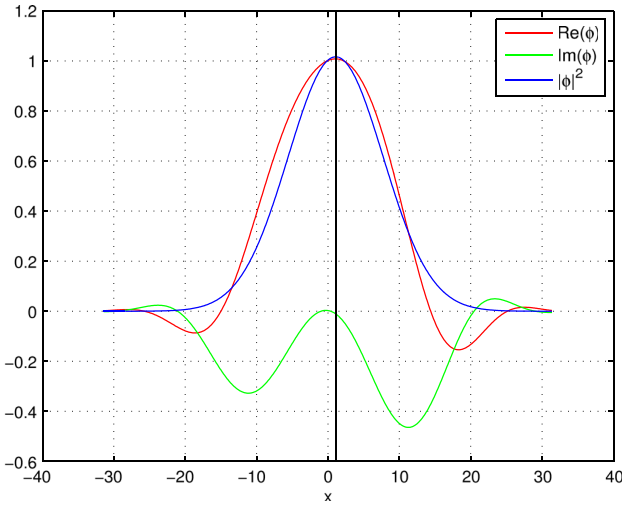

FIG. 5. The lowest order eigenfunction for a growing double resonant mode with $\hat{V}_E^{'} = 0.01$. The same plasma parameters as in Fig. 2 have been used with $\omega = -0.40 + i0.517$. The solid vertical line indicates the mode shift off the reference surface due to $\hat{V}_E^{'}$. Mode shift (ξ_{*k}) and width (Δ_k) are $\xi_{*k} = 1.085$ and $\Delta_k = 9.42$, respectively.

stabilization occurs when $k_y \gtrsim 0.65$. Figure 5 shows the lowest order eigenfunction for a growing mode with $\omega = -0.40 + i0.517$. Finite $\hat{V}_E^{'}$ increases the mode shift, as can be easily noticed in the figure.

IV. MOMENTUM FLUX IN THE VICINITY OF $r = r_{min}$

In this section, we calculate quasilinear parallel and poloidal momentum fluxes due to $E \times B$ and polarization drift in the vicinity of $r = r_{min}$. Assuming that $E \times B$ shearing rate is much smaller than the mode frequency, one can derive expressions for fluctuating parallel ($\delta v_{\parallel}$), poloidal (δv_y), and polarization (δv_{pol}) velocities as

$$\delta v_{\parallel} = \left(\frac{c_s \rho_s}{L_n}\right) \frac{k_y}{\omega} \left[-\hat{V}_{\parallel 0}^{'} + \frac{k_{\parallel}}{k_y}\left[1 - \frac{\omega_{*pi}}{\omega}\right]\right] \phi_k, \quad (27)$$

$$\delta v_y = i\left(\frac{c_s \rho_s}{L_n}\right) k_x \phi_k, \quad (28)$$

$$\delta v_{pol} = -c_s \left(\frac{\rho_s}{L_n}\right)^2 \omega k_x \phi_k, \quad (29)$$

respectively. Here, $\omega_{*pi} = -\tau_i \alpha_i k_y$, k_x is the radial wavenumber, $k_x = -i\partial \ln \phi_k / \partial x$, and ω is normalized to c_s/L_n, $\omega = \omega/(c_s/L_n)$. Then, it is straightforward to compute quasilinear momentum fluxes.

A. Spectral average and q-curvature driven momentum flux

Before embarking on actual calculations of momentum fluxes, we first consider the $\vec{k}$-space average of some quantity, such as $k_{\parallel}$, which is crucial to induce residual stress. This is an essential step to elucidate the origin of q-curvature driven intrinsic rotation by $\langle k_{\parallel} \rangle$ symmetry breaking, as will be shown shortly.

To proceed, we consider the $\vec{k}$-space summation of a quantity $Y(k_y, k_{||})$ weighted by turbulence intensity $|\phi_k|^2$

$$\langle Y\rangle \equiv \sum_{\vec{k}} Y(k_y,k_{||})|\phi_k|^2 = \sum_{k_y}\int dk_{||} Y(k_y,k_{||})|\phi_k|^2. \quad (30)$$

Using the definition of $k_{||}$ given in Eq. (2), one can convert, for a fixed k_z, the integral variable in Eq. (30) from $k_{||}$ to x giving rise to

$$\langle Y\rangle = -\frac{L_n}{q_0 R}\sum_{k_y}|k_y|\left(\langle Y(k_y,k_{||})\rangle_{\hat{s}} + \langle Y(k_y,k_{||}\rangle_{\hat{s}_d}\right), \quad (31)$$

where

$$\langle Y(k_y,k_{||})\rangle_{\hat{s}} = \hat{s}\int \mathrm{d}x Y(k_y,k_{||})|\phi_k|^2 \quad (32)$$

and

$$\langle Y(k_y,k_{||})\rangle_{\hat{s}_d} = 2\hat{s}_d\int \mathrm{d}x|x|Y(k_y,k_{||})|\phi_k|^2. \quad (33)$$

In Eqs. (31) and (33), we defined $\langle Y\rangle$ by using absolute values of k_y and x in order to make the summation/integration over $k_y(k_{||})$ easier. Note that $\langle Y(k_y,k_{||})\rangle_{\hat{s}_d}$ represents the pure q-curvature effect—it survives when $\hat{s}=0$.

Now, we consider the spectral average of $k_{||}$. One can immediately derive from Eq. (31) that

$$\langle k_{||}\rangle_{k_y} = -\frac{L_n}{q_0 R}|k_y|\left[\langle k_{||}\rangle_{\hat{s}} + \langle k_{||}\rangle_{\hat{s}_d}\right]. \quad (34)$$

The first term in the right hand side (RHS) of Eq. (34) is the net parallel wave momentum gain (i.e., intrinsic rotation) due to turbulence. For a symmetric eigenfunction with respect to $x=0$, this term becomes zero because $k_{||}\propto x$. Thus, some forms of symmetry breaking, such as $E\times B$ shear or finite ρ^* are necessary to generate intrinsic rotation out of this. The magnitude of $E\times B$ shear and ensuing mode shift determine the amount of intrinsic rotation generated by this term.

The second term is new in this paper. It represents the generation of net wave momentum due to generic magnetic configuration, i.e., q-curvature. Note that this term survives even when turbulence is symmetric about $x=0$. In other words, intrinsic rotation can be generated without invoking symmetry breaking when q-curvature is finite. The amount of net momentum generation is determined mainly by the width of modes (and amplitudes) in this case; broader modes yields larger intrinsic rotation.

The q-curvature driven parallel wave momentum generates intrinsic rotation in RS ITB. Thus, q-curvature can play as another source for intrinsic rotation, in addition to $E\times B$ shear driven symmetry breaking, the turbulence intensity gradient and profile shearing effect as pressure curvature. However, it must be mentioned that pressure curvature brings inhomogeneity in turbulence intensity and hence profile shearing effects should always be accompanied by turbulence intensity gradient effect. On the other hand, q-curvature may also affect turbulence intensity gradient though very weakly.[22] Since $\nabla V_{||}$ contribution to total $E\times B$ plays a crucial role in ITB formation, as shown in recent gyrofluid simulations,[39,40] the existence of intrinsic torque due to q-profile curvature will facilitate the barrier formation in RS plasmas. We also note the scaling $\langle k_{||}\rangle \propto \hat{s}_d$. This implies that strong RS configuration will provide stronger intrinsic torque which may play a role in expediting the ITB formation.

Similarly, one can evaluate the spectral average of k_x, which arises in the calculation of the poloidal Reynolds stress

$$\langle k_x\rangle_{k_y} = -\frac{L_n}{q_0 R}|k_y|\left[\langle k_x\rangle_{\hat{s}} + \langle k_x\rangle_{\hat{s}_d}\right]. \quad (35)$$

Again, finite q-curvature contributes to the generation of $\langle k_x\rangle$, hence the poloidal Reynolds stress, without invoking radial symmetry breaking of eigenmode structures. In Subsections IV B and IV C, we explicitly calculate parallel and poloidal Reynolds stresses coming from this q-curvature effect.

B. Parallel Reynolds stress

Using Eqs. (27) to (29), one can readily calculate the quasilinear parallel Reynolds stress

$$\begin{aligned}\Pi_{||} &= \Pi_{||}^{E} + \Pi_{||}^{pol}\\ &= \langle \delta v_{Ex}\delta v_{||}\rangle + \langle \delta v_{pol}\delta v_{||}\rangle\\ &= \left(\frac{c_s\rho_s}{L_n}\right)^2 \mathrm{Re}\sum_{\vec{k}} i\frac{k_y^2}{\omega}\left[-\hat{V}'_{||0} + \frac{k_{||}}{k_y}\left[1-\frac{\omega_{*pi}}{\omega}\right]\right]|\phi_k|^2, \quad (36)\\ &\quad + c_s^2\left(\frac{\rho_s}{L_n}\right)^3\left[\left\{\mathrm{Re}\sum_{\vec{k}}\left[\hat{V}'_{||0}k_x^* k_y - k_x^* k_{||}\left(1-\frac{\omega_{*pi}}{\omega}\right)\right]\right\}\right.\\ &\quad \left.\times|\phi_k|^2 - \frac{\partial}{\partial T}\left\langle\frac{\partial\phi}{\partial x}\delta v_{||}\right\rangle\right]. \quad (37)\end{aligned}$$

Here, $\Pi_{||}^{E}$ [Eq. (36)] and $\Pi_{||}^{pol}$ [Eq. (37)] are parallel Reynolds stresses driven by $E\times B$ and polarization drift, respectively. It will be instructive to explain the step leading to the last term in Eq. (37). $\Pi_{||}^{vpol}$ can be written as

$$\Pi_{||}^{pol} \sim \left\langle\frac{\partial\nabla_x\phi_k^*}{\partial t}\delta v_{||}\right\rangle \sim -\left\langle\nabla_x\phi_k^*\frac{\partial\delta v_{||}}{\partial t}\right\rangle + \frac{\partial}{\partial t}\langle\nabla_x\phi_k^*\delta v_{||}\rangle. \quad (38)$$

The first (second) term in the RHS of Eq. (38) corresponds to the first (second) term in Eq. (37). We use the capital "T" in the second term in Eq. (37) to denote that $\langle\nabla_x\phi_k^*\delta v_{||}\rangle$ varies slowly compared to mode frequency (i.e., in transport time scale). In steady states, this term becomes zero.

Equations (36) and (37) show that parallel momentum flux is decomposed of diffusive (i.e., being proportional to $\hat{V}'_{||}$) and residual (i.e., being independent of $\hat{V}_{||}$ and $\hat{V}'_{||}$) components. Let us first consider the diffusive component which

we denote by $\Pi_{\|}^{D}$. Using Eqs. (32), (33), (36), and (37), one can write $\Pi_{\|}^{D}$ as

$$\Pi_{\|}^{D} = -(\chi_{\|,E} + \chi_{\|,pol})\frac{dV_{\|0}}{dx}, \tag{39}$$

where

$$\chi_{\|,E} = -\left(\frac{c_s\rho_s}{L_n}\right)^2 \mathrm{Re}\sum_{k_y}\left(\frac{|k_y|L_n}{q_0R}\right) i\frac{k_y^2}{\omega}\left(\langle 1\rangle_{\hat{s}} + \langle 1\rangle_{\hat{s}_d}\right), \tag{40}$$

$$\chi_{\|,pol} = c_s^2\left(\frac{\rho_s}{L_n}\right)^3 \mathrm{Re}\sum_{k_y}\left(\frac{|k_y|L_n}{q_0R}\right) k_y\left[\langle \mathrm{Re}k_x^*\rangle_{\hat{s}} + \langle \mathrm{Re}k_x^*\rangle_{\hat{s}_d}\right] \tag{41}$$

are momentum diffusivity due to $E\times B$ and polarization drift, respectively.

Using the lowest order solution of the eigenfunction, Eq. (20), one can readily calculate $\langle 1\rangle_{\hat{s}}$ and $\langle 1\rangle_{\hat{s}_d}$, resulting in

$$\langle 1\rangle_{\hat{s}} = \hat{s}\Delta_k\sqrt{\pi}|\phi_{0k}|^2, \quad \langle 1\rangle_{\hat{s}_d} = 2\hat{s}_d\Delta_k^2|\phi_{0k}|^2. \tag{42}$$

Let us now calculate $\langle \mathrm{Re}k_x^*\rangle_{\hat{s}}$ and $\langle \mathrm{Re}k_x^*\rangle_{\hat{s}_d}$ using the lowest order eigenfunction. Since $\langle \mathrm{Re}k_x^*\rangle = \langle \mathrm{Re}k_x\rangle$, we calculate $\langle \mathrm{Re}k_x\rangle$. A straightforward calculation yields

$$\langle \mathrm{Re}k_x\rangle_{\hat{s}} = S_1\left[\langle x\rangle_{\hat{s}} + S_2\langle 1\rangle_{\hat{s}}\right], \tag{43}$$

$$\langle \mathrm{Re}k_x\rangle_{\hat{s}_d} = S_1\left[\langle x\rangle_{\hat{s}_d} + S_2\langle 1\rangle_{\hat{s}_d}\right], \tag{44}$$

with

$$\langle x\rangle_{\hat{s}} = \hat{s}\Delta_k\xi_k\sqrt{\pi}|\phi_{0k}|^2, \tag{45}$$

$$\langle x\rangle_{\hat{s}_d} = 4\hat{s}_d\Delta_k\xi_k\sqrt{\pi}|\phi_{0k}|^2, \tag{46}$$

$$S_1 = -\mathrm{Re}\sqrt{A_2}, \tag{47}$$

$$S_2 = \left(\mathrm{Re}\frac{A_1}{2A_2} - \frac{\mathrm{Im}\sqrt{A_2}}{\mathrm{Re}\sqrt{A_2}}\mathrm{Im}\frac{A_1}{2A_2}\right). \tag{48}$$

An interesting observation here is that finite $\hat{s}_d$ enhances the momentum diffusivity, scaling as Δ_k^2 in the lowest order. Thus, there is a competition between momentum generation due to residual stress, as will be described shortly, and the transport loss due to the enhancement of momentum diffusivity in the vicinity of $r = r_{min}$.

Now, we consider the non-diffusive parallel Reynolds stress, denoted by $\Pi_{\|}^{res}$. From Eqs. (36) and (37), one can write $\Pi_{\|}^{res}$ as

$$\begin{aligned}\Pi_{\|}^{res} &= \Pi_{\|,E}^{res} + \Pi_{\|,vpol}^{res} \\ &= \left(\frac{c_s\rho_s}{L_n}\right)^2 \mathrm{Re}\sum_{k_y}\left(-\frac{|k_y|L_n}{q_0R}\right) i\frac{k_y^2}{\omega}\left[1 - \frac{\omega_{*pi}}{\omega}\right] \\ &\quad\times\left\{\left\langle\frac{k_\|}{k_y}\right\rangle_{\hat{s}} + \left\langle\frac{k_\|}{k_y}\right\rangle_{\hat{s}_d}\right\} \\ &\quad + c_s^2\left(\frac{\rho_s}{L_n}\right)^3 \mathrm{Re}\sum_{k_y}\left(\frac{|k_y|L_n}{q_0R}\right) k_y\left[1 - \frac{\omega_{*pi}}{\omega}\right] \\ &\quad\times\left\{\langle k_x^* k_\|\rangle_{\hat{s}} + \langle k_x^* k_\|\rangle_{\hat{s}_d}\right\}.\end{aligned} \tag{49, 50}$$

Using the definition of $k_\|$ and the lowest order eigenfunction, the spectral averages appearing in Eq. (49) can be calculated in a similar way to the diffusive component, giving rise to

$$\left\langle\frac{k_\|}{k_y}\right\rangle_{\hat{s}} = \frac{k_z}{k_y}\langle 1\rangle_{\hat{s}} - \frac{L_n}{q_0R}\left[\hat{s}\langle x\rangle_{\hat{s}} + \hat{s}_d\langle x^2\rangle_{\hat{s}}\right], \tag{51}$$

$$\left\langle\frac{k_\|}{k_y}\right\rangle_{\hat{s}_d} = \frac{k_z}{k_y}\langle 1\rangle_{\hat{s}_d} - \frac{L_n}{q_0R}\left[\hat{s}\langle x\rangle_{\hat{s}_d} + \hat{s}_d\langle x^2\rangle_{\hat{s}_d}\right], \tag{52}$$

with

$$\langle x^2\rangle_{\hat{s}} = \hat{s}\left[\Delta_k^3\frac{\sqrt{\pi}}{2} + \Delta_k\xi_k^2\sqrt{\pi}\right]|\phi_{0k}|^2,$$

$$\langle x^2\rangle_{\hat{s}_d} = 2\hat{s}_d\left[\Delta_k^4 + 3\Delta_k^2\xi_k^2 + \Delta_k\xi_k^3\sqrt{\pi}\right]|\phi_{0k}|^2.$$

Equations (51) – (52) indicate two interesting points. First, $\Pi_{\|}^{res}$ can be generated without symmetry breaking (i.e., the radial asymmetry in eigenfunction), as manifested by the term $(k_z/k_y)\langle 1\rangle_{\hat{s}} = (k_z/k_y)\hat{s}\sqrt{\pi}\Delta_k|\phi_{0k}|^2$ in Eq. (51). However, this term is small because $\hat{s}\approx 0$ in the vicinity of $r = r_{min}$. Second, more importantly, finite q-curvature generates parallel wave momentum, as manifested by the term $(k_z/k_y)\langle 1\rangle_{\hat{s}_d}$ in Eq. (52).

To illustrate the significance of q-curvature driven residual stress in the absence of $E\times B$ shear, we present Fig. (6) where (a) $\langle k_\|/k_y\rangle$ and (b) parallel Reynolds stress ($\Pi_{\|}^{res}$) are plotted as a function of L_n/R. We take $V_E' = 0$, while keeping the ρ_s^* term. Thus, ρ_s^* is the only source for the symmetry breaking of eigenfunctions in this case. Solid lines correspond to $\langle k_\| k_y\rangle$ and $\Pi_{\|}^{res}$ without finite ρ_s^* effect, and dotted lines are those with the ρ_s^* term. As expected, $\Pi_{\|}^{res}$ decreases as L_n/R increases. One can also observe from Fig. 6 that $\Pi_{\|}^{res}$ due to finite ρ_s^* induced symmetry breaking is almost negligible in this particular case. Most contributions to $\Pi_{\|}^{res}$ come from the mode width through a quadratic dependence of $k_\|$

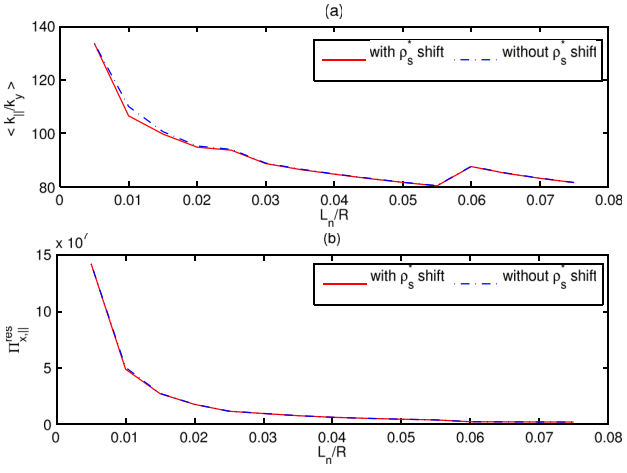

FIG. 6. (a) Spectral average of $k_\|/k_y$ and (b) parallel Reynolds stress ($\Pi_{x,\|}^{res}$) vs. L_n/R with (solid) and without (dot) ρ_s^* effect. Since $V_E' = 0$, ρ_s^* is the only source for the symmetry breaking of eigenfunctions in this case. $\Pi_{x,\|}^{res}$ due to the finite ρ_s^* induced symmetry breaking is almost negligible in this particular case, as can be seen in (a). Thus, most contributions to $\Pi_{x,\|}^{res}$ come from the q-curvature effect. $\Pi_{\|}^{res}$ decreases as L_n/R increases, as expected.

to x, i.e., $k_\parallel \propto x^2$. This q-curvature driven residual stress can provide the initial intrinsic rotation in RS plasmas, hence the seed $E\times B$ shear due to parallel flow shear, which may facilitate the ITB formation. After ITB formation, the intrinsic rotation will be dominated by the turbulence intensity gradient near the ITB head and the symmetry braking driven by strong $E\times B$ shear since $\gamma \lesssim V_E'$ in mature ITBs.

Similarly, one can compute the spectral average of $\langle k_x^* k_\parallel \rangle$ in a straightforward manner to calculate $\Pi^{res}_{\parallel,pol}$. The physical significance of $\Pi^{res}_{\parallel,pol}$ is that it survives, though smaller than $\Pi^{res}_{\parallel,E}$ to the order ρ_s/L_n, even without symmetry breaking because $k_\parallel \propto x$ and $k_x \propto x$. Here, it suffices to give the expression of $k_x^* k_\parallel$

$$k_x^* k_\parallel = A + Bx + Cx^2 + Dx^3,$$

where the coefficients A, B, C, and D are complex, in general, and are given by

$$A = k_z\left[\frac{i\xi_k}{\Delta_k^2} + S_1 S_2\right],$$

$$B = -k_z\left(\frac{i}{\Delta_k^2} - S_1\right) - \frac{k_y L_n \hat{s}}{q_0 R}\frac{A}{k_z},$$

$$C = \frac{k_y L_n \hat{s}}{q_0 R}\left[\left(\frac{i}{\Delta_k^2} - S_1\right) - \frac{i\xi_k}{\Delta_k^2} + \hat{s}_d \hat{s} S_1 S_2\right],$$

$$D = \frac{k_y L_n \hat{s}_d}{q_0 R}\left(\frac{i}{\Delta_k^2} - S_1\right),$$

with coefficients S_1 and S_2 given in Eqs. (47) and (48).

C. Poloidal Reynolds stress

Using Eq. (28), we can calculate the quasilinear poloidal Reynolds stress

$$\begin{aligned}\Pi_P &= \Pi_P^E + \Pi_P^{pol} \\ &= \langle \delta v_{Ex} \delta v_y \rangle + \langle \delta v_{pol} \delta v_y \rangle \\ &= \mathrm{Re}\sum_{k_y}\left(\frac{c_s\rho_s}{L_n}\right)^2 k_y \left(\frac{|k_y|L_n}{q_0 R}\right)\left[\mathrm{Re}\langle k_x\rangle \hat{s} + \mathrm{Re}\langle k_x\rangle_{\hat{s}_d}\right],\end{aligned} \tag{53}$$

$$-c_s^2\left(\frac{\rho_s}{L_n}\right)^3 \frac{\partial}{\partial T}\left[\frac{1}{2}\left\langle\left(\frac{\partial\phi}{\partial x}\right)^2\right\rangle\right]. \tag{54}$$

Here, Π_P^E and Π_P^{pol} are poloidal Reynolds stress driven by $E\times B$ and polarization drift, respectively. We first note that Π_P^{pol}, Eq. (54), varies slowly and becomes zero at steady states. So, we discuss Π_P only in this subsection. From Eq. (53), it is obvious that Π_P survives only when $\langle \mathrm{Re} k_x\rangle \neq 0$. Thus, standing eigenmodes with pure imaginary k_x cannot generate Π_P. Expressions for $\langle \mathrm{Re}k_x\rangle_{\hat{s}}$ and $\langle \mathrm{Re}k_x\rangle_{\hat{s}_d}$ corresponding to the lowest order eigenfunction are given in Eqs. (43) and (44), respectively, with relevant spectral averages and coefficients given in Eqs. (45)–(48).

To study the role of q-curvature in Π_P, we pay our attention to $r = r_{min}$ where $\hat{s} = 0$. Then, $\langle \mathrm{Re}k_x\rangle_{\hat{s}} = 0$ and only $\langle \mathrm{Re}k_x\rangle_{\hat{s}_d}$ survives. When the equilibrium parallel flow shear is low in the sense $-2k_z(Kk_y+\omega) \gg \omega k_y \hat{V}_\parallel'$ and $\hat{V}_E' = 0$, one can find that

$$S_1 = \frac{\gamma}{|\omega|^2}\sqrt{\frac{2|k_y k_z|\hat{s}_d L_n}{q_0 R}},$$
$$S_2 = 0.$$

This yields, in the lowest order,

$$\Pi_P = 4\sqrt{2\pi}\hat{s}_d^{3/2}\left(\frac{c_s\rho_s}{L_n}\right)^2 \mathrm{Re}\sum_{k_y} k_y \left(\frac{|k_y|L_n}{q_0 R}\right)^{3/2} \times \frac{\gamma |k_z|^{1/2}}{|\omega|^2}\Delta_k \xi_k |\phi_{0k}|^2. \tag{55}$$

One can make some interesting observations in Eq. (55). First, Π_P is induced only when k_z is finite. So, there will be no q-curvature driven poloidal momentum flux when $k_\parallel = 0$, i.e., when $r = r_{min}$ is a rational surface. In this sense, the double resonant modes or the non-resonant modes (i.e., modes that do not have rational surfaces for a given q profile) may effectively drive poloidal momentum flux. This effect, however, should be compensated more or less by the smallness of turbulence amplitude driven by these modes because of the Landau damping, which has not been considered in this paper. Second, Π_P requires the finite shift of an eigenmode. Since we assumed that $\hat{V}_E' = 0$, the only source for this mode shift is finite ρ^*, which is weak prior to ITB formation. However, this mean poloidal flow generation will increase as an ITB forms, due to the increase of $\hat{V}_E'$ and ρ^* resulting in the increase of ξ_k. This may accelerate the ITB formation process by providing poloidal flow contribution to total $E\times B$ shear. Of course, this poloidal momentum flux is to be balanced by neoclassical damping.

V. SUMMARY AND CONCLUSIONS

In this paper, we performed an analytic study, in the context of the quasilinear theory, of turbulent momentum transport in the vicinity of minimum q position in reversed magnetic shear configuration. Due to short temperature and density scale lengths at ITB at q-min in the reverse shear configuration the curvature effects become very weak. Also the toroidal mode coupling is weak in a small magnetic shear region around the qmin-surface. Moreover, a −ve magnetic shear strongly stabilizes toroidal ITG, while the slab ITG growth remains unaffected by sign change of magnetic shear. Hence, sheared slab ITG turbulence with the adiabatic electron response was considered in the presence of equilibrium shear flow. In particular, we focused on the role of finite q-curvature, which is generic in RS plasmas, in inducing turbulent parallel and poloidal Reynolds stresses. A summary of the main results in this paper is as follows:

- Finite q-curvature ($\hat{s}_d$) changes the eigenmode structure of the ITG mode in the vicinity of $r = r_{min}$ in RS configuration. Both the width (Δ_k) and the shift (ξ_k) of an eigenfunction are influenced by $\hat{s}_d$.

- Finite q-curvature can generically generate net parallel momentum without relying on asymmetry in eigenfunction. The origin of this parallel momentum generation lies in the relation $k_\parallel \propto \hat{s}_d x^2$. The amount of net momentum generated by the q-curvature effect is proportional to the width, rather than the shift off the rational surface, of the mode
- $\hat{s}_d$ enhances the parallel momentum diffusivity, resulting in deterioration of momentum confinement. This increase of outward momentum flux due to $\hat{s}_d$ is compensated by the $\hat{s}_d$-induced intrinsic rotation.
- Modes with finite $k_\parallel$ at $r = r_{min}$ can generate strong residual stress from finite $\hat{s}_d$. Intrinsic rotation generated by this novel effect should be taken into account in strong RS plasmas, in addition to externally injected momentum by NBI.
- A mean poloidal flow can be generated at $r = r_{min}$ by unstable modes with finite $k_\parallel$ and ξ_k. This poloidal flow can contribute to the total $E \times B$ flow shear at r_{min}, which may have an influence on ITB dynamics in RS plasmas.

The most important finding in this paper is that finite q-curvature plays an important role in momentum transport (both diffusive and non-diffusive) in the vicinity of $r = r_{min}$, where $\hat{s} \approx 0$. We pointed out that the residual stress and poloidal momentum flux driven by q-profile curvature may provide seed rotational shear (both in toroidal and poloidal) in ITB plasmas, possibly facilitating the ITB formation in RS configuration. However, it is unclear how the q-curvature driven momentum generation actually impact on RS ITB dynamics because our study is based on a quasi-linear analysis. In this regard, fully nonlinear gyrokinetic or gyrofluid simulations on this effect will be an interesting future subject.

It was shown that eigenmodes with finite k_z at r_{min} can effectively drive residual Reynolds stress. These modes correspond to double resonant modes which are excited when $q_{min} \neq m/n$ or non-resonant modes. In particular, we note that the presence of non-resonant modes have been attributed to hinder or hamper the ITB formation,[51] even though the physics of the role of nonresonant modes in ITB formation has not been fully elucidated and still remains an issue. This is another interesting issue to study in the future.

In this study, we did not consider Landau damping, which attenuates the mode amplitude with finite $k_\parallel$ at $r = r_{min}$. So, consideration of Landau damping will result in the reduction of q-profile curvature effect. However, main conclusions drawn in this paper will not be affected much even in the presence of Landaum damping, though some quantitative changes are expected.

It is likely that finite q-curvature effects will be significant in strong RS configuration. However, we point out that our analysis and main conclusions will still be applicable near the profile corner in weak or flat q-profiles where q-profile curvature is not negligible. In the flat q-region, there will be the competition between the reduction of turbulence amplitude due to the Landau damping and the increase of the mode width, which possibly makes our analysis still appreciable.

ACKNOWLEDGMENTS

R. Singh and R. Singh are thankful to Drs. Ö. D. Gürcan and H. Nordman for useful discussions. This work was supported by the French Agence nationale de la recherche, Contract No. ANR JCJC 0403 01, by the World Class Institute (WCI) Program of the National Research Foundation of Korea (NRF) funded by the Ministry of Science, ICT and Future Planning (NRF Grant No.: WCI 2009-001) and by the NFRI Internal Project under Grant No. EN 1306-1.

APPENDIX: A PERTURBATIVE CALCULATION OF EIGENFUNCTION AT $r = r_{min}$

In this Appendix, we present the first order correction of eigenvalues and eigenfunctions in Eq. (6) by keeping the quartic term in $U(x, \Omega)$, Eq. (2). For simplicity, we assume $\hat{s} = \hat{V}_E' = 0$. Then, using the same procedure in Sec. II, we obtain

$$\frac{d^2\Phi_k}{d\xi^2} + \left(E^* - \xi^2 + \frac{A_4}{(-A_2)^{3/2}}\xi^4\right)\Phi_k = 0. \tag{A1}$$

One can solve Eq. (A1) by treating the quartic term in $U(x, \Omega)$ perturbatively, similar to the time-independent perturbation theory in quantum mechanics

$$\phi = \sum_{n=0}^{\infty} \phi_n, \quad E = \sum_{n=0}^{\infty} E_n.$$

The lowest order solution of Eq. (A1) is given by

$$\Phi_0^l = \varphi_l H_l(\xi)\exp\left(-\frac{\xi^2}{2}\right), \qquad \varphi_l = (2^l l!\sqrt{\pi})^{-1/2}, \tag{A2}$$

with

$$E_0^{*l} = 2l + 1, \qquad l = 0, 1, 2, ... \tag{A3}$$

Then, the first order equation becomes

$$\left(\frac{\mathrm{d}^2}{\mathrm{d}\xi^2} + E_0^{*l} - \xi^2\right)\Phi_1^l + \left(E_1^{*l} + \frac{A_4}{(-A_2)^{3/2}}\xi^4\right)\Phi_0^l = 0. \tag{A4}$$

Taking $\Phi_1^l = \sum_m a_m^l \Phi_0^m$, multiplying Eq. (A4) by Φ_0^n and integrating over all ξ and using the property of self adjointness of the operator and orthogonality of the set $\{\Phi_0^l\}$, gives

$$\begin{aligned} a_n^l\left(E_0^{*l} - E_0^{*n}\right)2^n n! + E_1^{*l}\delta_{n,l}2^n n! + \frac{A_5}{(-A_3)^{3/2}}\left[2^{n-4}n!\delta_{n,l+4}\right. \\ + 2^{n-2}(2n-1)n!\delta_{n,l+2} + 3.2^{n-2}(2n^2+2n+1)n!\delta_{n,l+0} \\ \left. + 2^n(2n+3)(n+2)!\delta_{n,l-2} + 2^n(n+3)!\delta_{n,l-4}\right] = 0. \end{aligned} \tag{A5}$$

Setting $n = l$ in Eq. (A5) gives the solvability condition of Eq. (A4) which are nothing but the perturbed eigenvalues

$$E_1^{*l} = -\frac{A_5}{(-A_3)^{3/2}}[3.2^{-2}(2l^2+2l+1)]. \quad \text{(A6)}$$

Setting $n \neq l$ determines a_n^l,

$$a_n^l = -\frac{1}{E_0^{*l} - E_0^{*n}}\frac{A_5}{(-A_3)^{3/2}}\left[2^{n-4}n!\delta_{n,l+4} + 2^{n-2}(2n-1)n!\delta_{n,l+2} + 3.2^{n-2}(2n^2+2n+1)n!\delta_{n,l+0} + 2^n(2n+3)(n+2)!\delta_{n,l-2} + 2^n(n+3)!\delta_{n,l-4}\right]. \quad \text{(A7)}$$

The corrected eigenvalue up to the first order for $l=0$ radial quantum number is

$$E^{*0} = E_0^{*0} + E_1^{*0}, \quad \text{(A8)}$$

which gives the following dispersion relation:

$$-k_y^2 + \frac{1-\Omega}{K+\Omega} + \frac{k_z^2}{k_y^2\Omega^2} - \left(\frac{\rho_s^*}{2}\right)^2 = \frac{1}{k_y\Omega}\left\{\frac{2k_yk_z\hat{s}_dL_n}{q_0R}\right\}^{1/2} - \frac{3}{4}\left(\frac{k_y\hat{s}_dL_n}{2k_zq_0R}\right). \quad \text{(A9)}$$

The eigenfunction corrected up to the first order for $l=0$ radial quantum number is

$$\Phi^0 = \Phi_0^0 + a_2^0\Phi_0^2 + a_4^0\Phi_0^4. \quad \text{(A10)}$$

Substituting the value of coefficients a_n^l from Eq. (A7) in the above Eq. (A10) gives

$$\Phi^0 = \varphi_0\exp\left(-\frac{\xi^2}{2}\right) + \frac{A_5}{(-A_3)^{3/2}}\left[\varphi_2\frac{3}{16}(4\xi^2-2) + \varphi_4 2^{-7}(16\xi^4-48\xi^2+12)\right]\exp\left(-\frac{\xi^2}{2}\right), \quad \text{(A11)}$$

where $\varphi_n = (2^n n!\sqrt{\pi})^{-1/2}$. Thus, the total eigenfunction ϕ for the $l=0$ radial quantum number, including the ρ_s^* effect, becomes

$$\phi^0 = \varphi_0\exp\left(-\frac{\xi^2}{2} + \frac{1}{2}(-A_3)^{-1/4}\rho_s^*\xi\right) + \frac{A_5}{(-A_3)^{3/2}} \times \left[\varphi_2\frac{3}{16}(4\xi^2-2) + \varphi_4 2^{-7}(16\xi^4-48\xi^2+12)\right] \times \exp\left(-\frac{\xi^2}{2} + \frac{1}{2}(-A_3)^{-1/4}\rho_s^*\xi\right). \quad \text{(A12)}$$

[1]H. Biglari, P. H. Diamond, and P. W. Terry, Phys. Fluids B **2**, 1 (1990).
[2]T. S. Hahm and K. H. Burrell, Phys. Plasmas **2**, 1648 (1995).
[3]A. Bondeson and D. J. Ward, Phys. Rev. Lett. **72**, 2709 (1994).
[4]A. M. Garofalo, A. D. Turnbull, M. E. Austin, J. Bialek, M. S. Chu, K. J. Comer, E. D. Fredrickson, R. J. Groebner, R. J. La Haye, L. L. Lao, E. A. Lazarus, G. A. Navratil, T. H. Osborne, B. W. Rice, S. A. Sabbagh, J. T. Scoville, E. J. Strait, and T. S. Taylor, Phys. Rev. Lett. **82**, 3811 (1999).
[5]K. C. Shaing, Phys. Rev. Lett. **86**, 640 (2001).
[6]B. Coppi, Nucl. Fusion **42**, 1 (2002).
[7]P. H. Diamond, C. J. McDevitt, Ö. D. Gürcan, T. Hahm, W. X. Wang, E. Yoon, I. Holod, Z. Lin, V. Naulin, and R. Singh, Nucl. Fusion **49**, 045002 (2009).
[8]P. H. Diamond, C. J. McDevitt, Ö. D. Gürcan, T. S. Hahm, and V. Naulin, Phys. Plasmas **15**, 012303 (2008).
[9]T. S. Hahm, P. H. Diamond, O. D. Gurcan, and G. Rewoldt, Phys. Plasmas **14**, 072302 (2007).
[10]R. E. Waltz, G. M. Staebler, J. Candy, and F. L. Hinton, Phys. Plasmas **14**, 122507 (2007).
[11]Ö. D. Gürcan, P. H. Diamond, and T. S. Hahm, Phys. Rev. Lett. **100**, 135001 (2008).
[12]E. S. Yoon and T. S. Hahm, Nucl. Fusion **50**, 064006 (2010).
[13]A. G. Peeters, C. Angioni, and D. Strintzi, Phys. Rev. Lett. **98**, 265003 (2007).
[14]N. Kluy, C. Angioni, Y. Camenen, and A. G. Peeters, Phys. Plasmas **16**, 122302 (2009).
[15]R. R. Dominguez and G. M. Staebler, Phys. Fluids B **5**, 3876 (1993).
[16]X. Garbet, Y. Sarazin, P. Ghendrih, S. Benkadda, P. Beyer, C. Figarella, and I. Voitsekhovitch, Phys. Plasmas **9**, 3893 (2002).
[17]A. G. Peeters, C. Angioni, and the ASDEX Upgrade Team, Phys. Plasmas **12**, 072515 (2005).
[18]Ö. D. Gürcan, P. H. Diamond, T. S. Hahm, and R. Singh, Phys. Plasmas **14**, 042306 (2007).
[19]O. D. Gürcan, P. H. Diamond, P. Hennequin, C. J. McDevitt, X. Garbet, and C. Bourdelle, Phys. Plasmas **17**, 112309 (2010).
[20]S. Ku, J. Abiteboul, P. Diamond, G. Dif-Pradalier, J. Kwon, Y. Sarazin, T. Hahm, X. Garbet, C. Chang, G. Latu, E. Yoon, P. Ghendrih, S. Yi, A. Strugarek, W. Solomon, and V. Grandgirard, Nucl. Fusion **52**, 063013 (2012).
[21]W. X. Wang, T. S. Hahm, S. Ethier, G. Rewoldt, W. W. Lee, W. M. Tang, S. M. Kaye, and P. H. Diamond, Phys. Rev. Lett. **102**, 035005 (2009).
[22]J. Kwon, S. Yi, T. Rhee, P. Diamond, K. Miki, T. Hahm, J. Kim, Ö. Gürcan, and C. McDevitt, Nucl. Fusion **52**, 013004 (2012).
[23]F. J. Casson, A. G. Peeters, Y. Camenen, W. A. Hornsby, A. P. Snodin, D. Strintzi, and G. Szepesi, Phys. Plasmas **16**, 092303 (2009).
[24]Y. Camenen, A. G. Peeters, C. Angioni, F. J. Casson, W. A. Hornsby, A. P. Snodin, and D. Strintzi, Phys. Rev. Lett. **102**, 125001 (2009).
[25]Y. Camenen, A. G. Peeters, C. Angioni, F. J. Casson, W. A. Hornsby, A. P. Snodin, and D. Strintzi, Phys. Plasmas **16**, 062501 (2009).
[26]R. E. Waltz, G. M. Staebler, and W. M. Solomon, Phys. Plasmas **18**, 042504 (2011).
[27]Y. Camenen, Y. Idomura, S. Jolliet, and A. Peeters, Nucl. Fusion **51**, 073039 (2011).
[28]J. Weiland, R. Singh, H. Nordman, P. Kaw, A. Peeters, and D. Strinzi, Nucl. Fusion **49**, 065033 (2009).
[29]C. J. McDevitt, P. Diamond, and O. Gurcan, Phys. Rev. Lett. **103**, 205003 (2009).
[30]C. J. McDevitt, P. Diamond, O. Gurcan, and T. Hahm, Phys. Plasmas **16**, 052302 (2009).
[31]R. Singh, R. Ganesh, R. Singh, P. Kaw, and A. Sen, Nucl. Fusion **51**, 013002 (2011).
[32]R. Singh, R. Singh, P. Kaw, P. H. Diamond, O. D. Gurcan, and H. Nordman, Phys. Plasmas **19**, 012301 (2012).
[33]A. Peeters, C. Angioni, A. Bortolon, Y. Camenen, F. Casson, B. Duval, L. Fiederspiel, W. Hornsby, Y. Idomura, T. Hein, N. Kluy, P. Mantica, F. Parra, A. Snodin, G. Szepesi, D. Strintzi, T. Tala, G. Tardini, P. de Vries, and J. Weiland, Nucl. Fusion **51**, 094027 (2011).
[34]C. Angioni, Y. Camenen, F. Casson, E. Fable, R. McDermott, A. Peeters, and J. Rice, Nucl. Fusion **52**, 114003 (2012).
[35]P. Diamond, Y. Kosuga, Ö. Gürcan, C. McDevitt, T. Hahm, N. Fedorczak, J. Rice, W. Wang, S. Ku, J. Kwon, G. Dif-Pradalier, J. Abiteboul, L. Wang, W. Ko, Y. Shi, K. Ida, W. Solomon, H. Jhang, S. Kim, S. Yi, S. Ko, Y. Sarazin, R. Singh, and C. Chang, Nucl. Fusion **53**, 104019 (2013).
[36]J. E. Rice, Y. A. Podpaly, M. L. Reinke, R. Mumgaard, S. D. Scott, S. Shiraiwa, G. M. Wallace, B. Chouli, C. Fenzi-Bonizec, M. F. F. Nave, P. H. Diamond, C. Gao, R. S. Granetz, J. W. Hughes, R. R. Parker, P. T. Bonoli, L. Delgado-Aparicio, L.-G. Eriksson, C. Giroud, M. J. Greenwald, A. E. Hubbard, I. H. Hutchinson, J. H. Irby, K. Kirov, J. Mailloux, E. S. Marmar, and S. M. Wolfe, Phys. Rev. Lett. **111**, 125003 (2013).
[37]M. E. Austin, K. H. Burrell, R. E. Waltz, K. W. Gentle, P. Gohil, C. M. Greenfield, R. J. Groebner, W. W. Heidzardnk, Y. Luo, J. E. Kinsey, M. A. Makowski, G. R. McKee, R. Nazikian, C. C. Petty, R. Prater, T. L. Rhodes, M. W. Shafer, and M. A. V. Zeeland, Phys. Plasmas **13**, 082502 (2006).

[38]C. Fiore, J. E. Rice, Y. Podpaly, I. Bespamyatnov, W. Rowan, J. Hughes, and M. Reinke, Nucl. Fusion **50**, 064008 (2010).
[39]S. Kim, H. Jhang, P. Diamond, L. Terzolo, S. Yi, and T. Hahm, Nucl. Fusion **51**, 073021 (2011).
[40]H. Jhang, S. S. Kim, and P. H. Diamond, J. Korean Phys. Soc. **61**, 55 (2012).
[41]J. Y. Kim, Y. Kishimoto, M. Wakatani, and T. Tajima, Phys. Plasmas **3**, 3689 (1996).
[42]Y. Kishimoto, J. Y. Kim, W. Horton, T. Tajima, M. J. LeBrun, and S. Shirai, Plasma Phys. Controlled Fusion **40**, A663 (1999).
[43]Y. Kishimoto, J. Y. Kim, W. Horton, T. Tajima, M. J. LeBrun, S. A. Dettrick, J. Q. Li, and S. Shirai, Nucl. Fusion **40**, 667 (2000).
[44]C. Kessel, J. Manickam, G. Rewoldt, and W. M. Tang, Phys. Rev. Lett. **72**, 1212 (1994).
[45]J. Y. Kim and M. Wakatani, Phys. Plasmas **2**, 1012–1014 (1995).
[46]S. Brunner, M. Fivaz, T. M. Tran, and J. Vaclavik, Phys. Plasmas **5**, 3929–3949 (1998).
[47]J. Li, Y. Kishimoto, and T. Tuda, Plasma Phys. Controlled Fusion **42**, 443 (2000).
[48]L. Bai, A. Fukuyama, and M. Uchida, Phys. Plasmas **5**, 989 (1998).
[49]J. Q. Li, L. Huang, and W. X. Qu, Phys. Plasmas **5**, 959 (1998).
[50]S. Tokunaga, H. Jhang, S. S. Kim, and P. H. Diamond, Phys. Plasmas **19**, 092303 (2012).
[51]J. Candy, R. E. Waltz, and M. N. Rosenbluth, Phys. Plasmas **11**, 1879 (2004).